Ann. Geophys., 34, 55–65, 2016
www.ann-geophys.net/34/55/2016/
doi:10.5194/angeo-34-55-2016

Annales Geophysicae Open Access EGU

Mapping of steady-state electric fields and convective drifts in geomagnetic fields – Part 1: Elementary models

A. D. M. Walker[1] **and G. J. Sofko**[2]

[1]School of Chemistry and Physics, University of KwaZulu-Natal, Durban, South Africa
[2]Institute of Space and Atmospheric Studies, University of Saskatchewan, Saskatchewan, Canada

Correspondence to: A. D. M. Walker (walkerd@ukzn.ac.za)

Received: 26 October 2015 – Revised: 13 December 2015 – Accepted: 17 December 2015 – Published: 19 January 2016

Abstract. When studying magnetospheric convection, it is often necessary to map the steady-state electric field, measured at some point on a magnetic field line, to a magnetically conjugate point in the other hemisphere, or the equatorial plane, or at the position of a satellite. Such mapping is relatively easy in a dipole field although the appropriate formulae are not easily accessible. They are derived and reviewed here with some examples. It is not possible to derive such formulae in more realistic geomagnetic field models. A new method is described in this paper for accurate mapping of electric fields along field lines, which can be used for any field model in which the magnetic field and its spatial derivatives can be computed. From the spatial derivatives of the magnetic field three first order differential equations are derived for the components of the normalized element of separation of two closely spaced field lines. These can be integrated along with the magnetic field tracing equations and Faraday's law used to obtain the electric field as a function of distance measured along the magnetic field line. The method is tested in a simple model consisting of a dipole field plus a magnetotail model. The method is shown to be accurate, convenient, and suitable for use with more realistic geomagnetic field models.

Keywords. Ionosphere (ionosphere-magnetosphere interactions; instruments and techniques) – magnetospheric physics (instruments and techniques)

1 Introduction

In studies of magnetospheric convection, such as those by the SuperDARN network (Greenwald et al., 1995), the mapping of electric fields along magnetic field lines to the location of satellites on the same field line or the conjugate point in the ionosphere in the opposite hemisphere is of considerable importance. Except in the neighbourhood of strong auroral activity it can be assumed that the parallel conductivity is infinite so that for large-scale electric fields that are electrostatic on the timescale of interest, the magnetic field lines are equipotentials. For a dipole magnetic field, the mapping is easy, although, surprisingly, techniques for doing so are not explicitly covered in elementary texts on magnetosphere physics. For more realistic models of the magnetosphere where the magnetic field lines are stretched, as they are for lines reaching the magnetic equator at distances r_0 beyond geostationary orbit, the problem of mapping can become quite complex.

Most mapping has been done by concentrating on the electric potential. For an electrostatic field the magnetic field lines are equipotentials. If the field is required several magnetic field lines are traced and their separation calculated. From their separation the gradient of the electric potential is estimated to give the electric field. Examples of this approach are in Lyons and Williams (1984, chapter 2) for a dipole field and Baker et al. (2004) for a more general field. This is inherently inaccurate, requiring the evaluation of a small difference of large quantities. For example, the typical length of an auroral latitude field line is 10^5 km. If we compare electric fields at the conjugate points in the ionosphere by considering two field lines separated by 10 km at the ground, then in order to achieve 10 % accuracy (1 km) in the field line separation at the conjugate point the arrival points of the two adjacent field lines must be computed to 1 part in 10^5.

This paper presents a new technique that can directly compute the electric field mapping in any geomagnetic field model provided that the magnetic field and its spatial deriva-

tives are given at all points of interest. Provided that the magnetosphere is in a steady state, the electric field mapping is a straightforward application of Faraday's law. If the element of separation of two field lines can be calculated as a function of position on the field line, then, since the field lines are equipotentials, the electric field can be calculated. Since the separation is calculated by integrating an analytic formula along with the field line, its accuracy is the same as that of the field line position.

It is, however, also very useful to have as a reference the expected mapping for a purely dipole field. The derivation of expressions for mapping in a dipole field is straightforward, but, surprisingly, no convenient collection of the relevant formulae seems to be available. Mozer (1970) has provided formulae for the special case of mapping the ionospheric electric field to the dipole equatorial plane but not the more general formulae. There appears to be no simple published version of the actual mapping of the components of $\boldsymbol{E}$ and of the components of the convective drift between conjugate points along dipole field lines.

We therefore first provide an easily accessible derivation of a number of relevant formulae for a dipole field. They are useful for tutorial purposes and provide analytic expressions for validating the new tensor field mapping techniques. These mappings are used for some illustrative examples which give rough estimates of how electric fields and convective drifts vary with altitude. For example, we make comparisons between convective drifts measured by the DMSP satellites at about 840 km altitude and SuperDARN F-region measurements in the 250–325 km altitude range, for L values of about 6.6 and lower. For $L \sim 6.6$, these comparisons should normally show that the DMSP measurements should be about 14 % greater, simply because of the mapping of the convective drift from the F-region to DMSP altitude.

Finally we introduce a new method in which a second rank tensor is analytically derived which satisfies a set of first order differential equations. This tensor provides a measure of the divergence and convergence of the field lines and can be found by a step-by-step integration of the differential equations simultaneously with the tracing of the magnetic field line. This can be used to deduce the electric field without the inaccuracies inherent in the method used, inter alia, by Baker et al. (2004). The method is tested for a simple model consisting of a dipole field with a Harris (1962) current sheet to simulate the magnetotail.

2 Mapping in a dipole field

2.1 Basic ideas

All mapping techniques depend on the same principle. Except where there are electric fields parallel to $\boldsymbol{B}$, for example near auroral arcs, the magnetic field lines are equipotentials. We may write Faraday's law in the form

$$\oint \boldsymbol{E} \cdot \mathrm{d}\boldsymbol{l} = 0 \tag{1}$$

provided that the timescales on which changes take place is longer than the Alfvén transit time so that the magnetic induction $\mathrm{d}\Phi/\mathrm{d}t$ can be ignored. If we then consider a contour bounded by two adjacent field lines and terminated at each end by line segments $\delta\boldsymbol{w}$ normal to $\boldsymbol{B}$ then there is no contribution to the integral from the portion of the contour coinciding with the field lines. Then if E_1 is the component of the electric field parallel to w_1 and E_2 that parallel to w_2, (Eq. 1) becomes

$$E_1 \delta w_1 - E_2 \delta w_2 = 0 \tag{2}$$

or

$$\frac{E_1}{E_2} = \frac{\delta w_2}{\delta w_1}. \tag{3}$$

Thus we simply need to find how $\delta\boldsymbol{w}$ changes along the field lines and the electric field component along it is inversely proportional to its magnitude. Equivalently, the magnetic field lines lie on electric equipotentials so that the electric field is perpendicular to the magnetic field. If we consider two closely spaced magnetic field lines separated by perpendicular distance δw and having an electric potential difference $\delta\Phi$ then the component of the electric field parallel to δw is given by

$$E = -\lim_{\delta w \to 0} \frac{\delta\Phi}{\delta w} \propto \frac{1}{\delta w}. \tag{4}$$

Mozer (1970) gives expressions for the mapping of the electric field between the ionosphere and the equatorial plane:

$$\frac{E_{\mathrm{Mi}}}{E_{\mathrm{Me}}} = 2L\sqrt{L - \frac{3}{4}} \tag{5}$$

$$\frac{E_{\mathrm{Wi}}}{E_{\mathrm{We}}} = L^{3/2}, \tag{6}$$

where E_M is the component of the electric field perpendicular to $\boldsymbol{B}$ in the meridian plane and E_{W} is the westward component. The subscripts i and e refer to the values at the ionosphere and the equatorial plane, although actually the formulae are calculated as if the ionosphere was at zero altitude. We shall generalize these to apply to the mapping between any two points on a magnetic field line.

2.2 Dipole field geometry

We shall map the electric field components in a simple centred magnetic dipole field. Expressions describing the dipole field and its geometry are given, for example, by Walker (2005, Appendix B). The geometry near the surface of the

Earth is shown in Fig. 1. We can use a spherical polar system with the axis coincident with the dipole axis. Rather than polar angle we use its complement, the magnetic latitude. This is not the same as the magnetic latitude defined in realistic models of the magnetic field.

The field is given as a function of position by

$$\boldsymbol{B} = \frac{B_{\rm eq} R_{\rm E}^3}{r^3}\left\{-2\hat{\boldsymbol{r}}\sin\lambda + \hat{\boldsymbol{\lambda}}\cos\lambda\right\}, \tag{7}$$

where the unit vectors are along the radial and latitudinal directions, $\boldsymbol{B}_{\rm eq}$ is the field at the surface of the earth at the equator ($\sim 3.154\times10^{-5}T$), $R_{\rm E}$ is the Earth's radius (~ 6378 km), λ is the magnetic latitude, and r is the radial distance from the Earth's centre.

The equation of a dipole field line is

$$r = R_{\rm E} L \cos^2\lambda, \tag{8}$$

where L is the radial distance at which the field line crosses the equator, measured in Earth radii. The radius r can be eliminated from Eqs. (7) and (8) to give $\boldsymbol{B}$ as a function of λ on the field line defined by the parameter L:

$$\boldsymbol{B} = \frac{B_0\left\{-2\hat{\boldsymbol{r}}\sin\lambda + \hat{\boldsymbol{\lambda}}\cos\lambda\right\}}{\cos^6\lambda}, \tag{9}$$

where B_0, the value of B at the apex of the field line is

$$B_0 = B_{\rm eq}/L^3. \tag{10}$$

The magnitude of the magnetic field as a function of latitude on the field line is then

$$B = \frac{B_0\sqrt{1+3\sin^2\lambda}}{\cos^6\lambda}. \tag{11}$$

The magnetic field lines lie in the magnetic meridian plane, in which the unit vector parallel to the magnetic field is given by

$$\hat{\boldsymbol{\mu}} = \frac{-2\hat{\boldsymbol{r}}\sin\lambda + \hat{\boldsymbol{\lambda}}\cos\lambda}{\sqrt{1+3\sin^2\lambda}}. \tag{12}$$

The unit outward normal vector in the meridian plane is given by

$$\hat{\boldsymbol{\nu}} = \frac{\hat{\boldsymbol{r}}\cos\lambda + 2\hat{\boldsymbol{\lambda}}\sin\lambda}{\sqrt{1+3\sin^2\lambda}}. \tag{13}$$

We complete the right-handed system with a unit vector $\hat{\boldsymbol{\phi}}$ normal to the meridian plane in the easterly direction. The right-handed coordinate system is defined by the vectors $\hat{\boldsymbol{\mu}}, \hat{\boldsymbol{\nu}}, \hat{\boldsymbol{\phi}}$, in that order. This system of local coordinates is easily generalized to situations where the field lines do not lie in a plane. The directions of the unit vectors are shown in Fig. 1. The grid at the bottom of the figure shows lines of latitude and longitude at the Earth's surface.

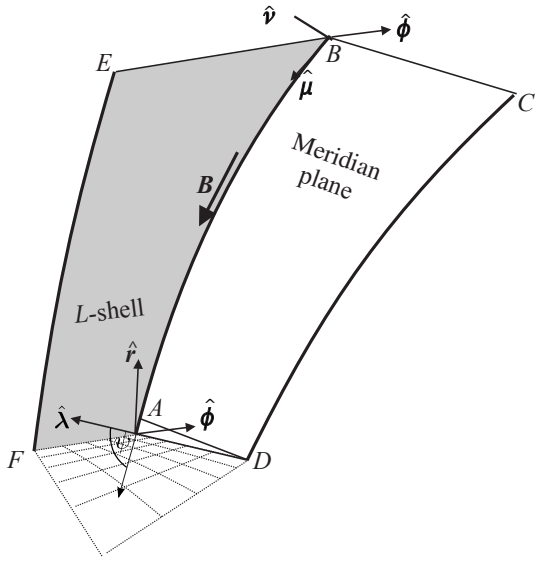

Figure 1. Dipole field: directions of unit vectors.

The figure also shows the unit vectors $\hat{\boldsymbol{r}}$ in the radial direction and $\hat{\boldsymbol{\lambda}}$ in the direction of increasing latitude. The angle between $\hat{\boldsymbol{\lambda}}$ and $\hat{\boldsymbol{\mu}}$ is the dip angle ψ, as is the angle between $\hat{\boldsymbol{r}}$ and $\hat{\boldsymbol{\nu}}$. Thus

$$\cos\psi = \hat{\boldsymbol{\lambda}}\cdot\hat{\boldsymbol{\mu}} = \hat{\boldsymbol{r}}\cdot\hat{\boldsymbol{\nu}} \tag{14}$$

and from Eqs. (12) or (13)

$$\cos\psi = \frac{\cos\lambda}{\sqrt{1+3\sin^2\lambda}}. \tag{15}$$

The element of perpendicular distance between two field lines that lie in the meridian plane is

$$\delta w_\nu = \delta r\cos\psi. \tag{16}$$

The element δr is the radial length element at constant λ so that, from (Eq. 8),

$$\delta r = \left(\frac{\partial r}{\partial L}\right)_\lambda \delta L = R_{\rm E}\cos^2\lambda\,\delta L. \tag{17}$$

Thus

$$\delta w_\nu = \frac{R_{\rm E}\cos^3\lambda}{\sqrt{1+3\sin^2\lambda}}\,\delta L. \tag{18}$$

The perpendicular distance between two closely spaced field lines that lie in the same L-shell, expressed in terms of the difference $\delta\phi$ in longitude is $r\cos\lambda\,\delta\phi$. From the field line equation this can be expressed in terms of the latitude:

$$\delta w_\phi = L R_{\rm E}\cos^3\lambda\delta\phi. \tag{19}$$

Sometimes we need to consider a horizontal path between the field lines L and $L+\delta L$. At a fixed radius r Eq. (8) for a field line can be differentiated, keeping r constant, to obtain

$$0 = R_{\rm E}\cos^2\lambda\,\delta L - 2R_{\rm E}L\sin\lambda\cos\lambda\,\delta\lambda \tag{20}$$

so that, at any fixed radius r and latitude λ, the change in L in moving to a neighbouring field line at $\lambda+\delta\lambda$ is

$$\delta L = 2L\tan\lambda\,\delta\lambda. \tag{21}$$

If we assume that there are no potential drops along the magnetic field lines, then there can be no component of the electric field parallel to the magnetic field, and therefore can only have components along $\hat{\boldsymbol{\nu}}$ and $\hat{\boldsymbol{\phi}}$, so we can write

$$\boldsymbol{E} = \hat{\boldsymbol{\nu}}E_\nu + \hat{\boldsymbol{\phi}}E_\phi. \tag{22}$$

Since $\hat{\boldsymbol{\nu}}E_\nu = \hat{\boldsymbol{r}}E_r + \hat{\boldsymbol{\lambda}}E_\lambda$, from Eq. (13) we get

$$E_r = \frac{\cos\lambda}{\sqrt{1+3\sin^2\lambda}}E_\nu \tag{23}$$

$$E_\lambda = \frac{2\sin\lambda}{\sqrt{1+3\sin^2\lambda}}E_\nu \tag{24}$$

and thus E_r and E_λ are related by

$$E_r = \frac{1}{2}E_\lambda\cot\lambda. \tag{25}$$

The mapping of the perpendicular components of the electric field is now straightforward. We specify a point on the field line by its latitude λ. Then from the general mapping relation (Eq. 2) and the expression (Eq. 18) the ratio between the ν-components of the electric field at two different latitudes is

$$\frac{E_{\nu 1}}{E_{\nu 2}} = \frac{\cos^3\lambda_2}{\cos^3\lambda_1}\sqrt{\frac{1+3\sin^2\lambda_1}{1+3\sin^2\lambda_2}} \tag{26}$$

and from Eq. (19) that between the ϕ components is

$$\frac{E_{\phi 1}}{E_{\phi 2}} = \frac{\cos^3\lambda_2}{\cos^3\lambda_1}. \tag{27}$$

There are two closed paths we shall use for Eq. (1). First, we integrate in the meridian plane between an ionospheric segment at a fixed altitude r = constant, then along the field line labelled L (where $LR_{\rm E}$ is the radial distance at which the line reaches the equator), then radially outward from $LR_{\rm E}$ to $(L+\delta L)R_{\rm E}$ and finally back along the field line to the ionosphere, as shown in Fig. 2. Then (Eq. 1) becomes

$$E_\lambda\, r\,\delta\lambda = E_{r,\rm eq}R_{\rm E}\,\delta L. \tag{28}$$

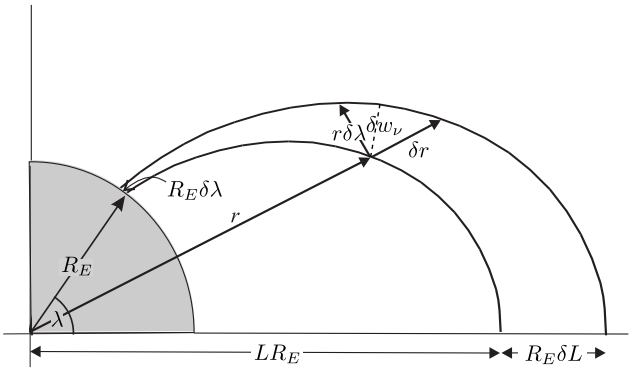

Figure 2. Dipole field: meridian plane.

Then Eqs. (8), (21), and (28) can be used to show that

$$E_{r,0} = \frac{\cos^3\lambda}{2\sin\lambda}E_\lambda, \tag{29}$$

where the subscript 0 refers to the value at the apex of the field line.

We can eliminate E_λ from Eq. (24) and (29) to obtain E_ν in terms of $E_{r,0}$

$$E_\nu = \frac{\sqrt{1+3\sin^2\lambda}}{\cos^3\lambda}E_{r,0}. \tag{30}$$

The total field can then be written

$$\boldsymbol{E} = \frac{\hat{\boldsymbol{r}}\cos\lambda E_{r,0} + 2\hat{\boldsymbol{\lambda}}\sin\lambda E_{r,0} + \hat{\boldsymbol{\phi}}E_{\phi,0}}{\cos^3\lambda}. \tag{31}$$

2.3 Mapping the convective drift

The convective or Hall drift is given by

$$\boldsymbol{v}_H = \frac{\boldsymbol{E}\times\boldsymbol{B}}{B^2} = \frac{\hat{\boldsymbol{\nu}}E_\phi - \hat{\boldsymbol{\phi}}E_\nu}{B}, \tag{32}$$

which gives the convective (Hall) drift in terms of the two E-vector components perpendicular to $\boldsymbol{B}$. From Eqs. (30) and (27) this becomes

$$\boldsymbol{v}_H = \frac{\hat{\boldsymbol{\nu}}E_{\phi,0}\cos^3\lambda}{B_0\sqrt{1+3\sin^2\lambda}}\frac{\hat{\boldsymbol{\phi}}E_{r,0}\cos^3\lambda}{B_0}. \tag{33}$$

We can take the cross product of $\boldsymbol{E}$ and $\boldsymbol{B}$ given by Eqs. (7) and (31) to express the drift in spherical polar coordinates

$$\boldsymbol{v}_H = \frac{\hat{\boldsymbol{r}}E_{\phi,0}\cos^4\lambda}{B_0(1+3\sin^2\theta)} + \frac{2\hat{\boldsymbol{\lambda}}E_{\phi,0}\sin\lambda\cos^3\lambda}{B_0(1+3\sin^2\lambda)} \frac{\hat{\boldsymbol{\phi}}E_{r,0}\cos^3\lambda}{B_0}. \tag{34}$$

Equations (33) and (31) can be used to find the ratios of the convective flow values at two conjugate points (r_1,λ_1)

and (r_2, λ_2). From Eq. (33), the meridian plane convective velocity component ratio is

$$\frac{v_{\nu,2}}{v_{\nu,1}} = \frac{\cos^3\lambda_2}{\cos^3\lambda_1}\sqrt{\frac{1+3\sin^2\lambda_1}{1+3\sin^2\lambda_2}} = \left(\frac{r_2}{r_1}\right)^{3/2}\sqrt{\frac{4L-3r_1/R_\mathrm{E}}{4L-3r_2/R_\mathrm{E}}} \quad (35)$$

and the eastward velocity component ratio is

$$\frac{v_{\phi,2}}{v_{\phi,1}} = \frac{\cos^3\lambda_2}{\cos^3\lambda_1} = \left(\frac{r_2}{r_1}\right)^{3/2}. \quad (36)$$

Consider as an example the mapping from the ionosphere to a DMSP satellite. Table 1 gives the ratios of the velocity components for mapping along field lines of varying L from an ionospheric height h_1 to DMSP at an assumed altitude h_2 of 840 km, using $R_\mathrm{E} = 6378$ km.

2.4 Cross-section of a magnetic flux tube

Since $\hat{\boldsymbol{\nu}}$ and $\hat{\boldsymbol{\phi}}$ are mutually perpendicular, and both are normal to $\boldsymbol{B}$, the element of cross-sectional area of a flux tube is

$$\delta\boldsymbol{A} = \hat{\boldsymbol{\nu}}\delta w_\nu \times \hat{\boldsymbol{\phi}}\delta w_\phi = \hat{\boldsymbol{\mu}}\delta w_\nu \delta w_\phi \quad (37)$$

We use Eqs. (18) and (19) to show that

$$\delta A = \frac{L R_\mathrm{E}^2 \cos^6\lambda}{\sqrt{1+3\sin^2\lambda}}\delta L \delta\phi \quad (38)$$

so that, using Eq. (11)

$$B\delta A = B_\mathrm{eq} R_\mathrm{E}^2 L \delta\phi \delta L = B_0 \delta A_0 \quad (39)$$

expressing the conservation of magnetic flux along a field line. This is, of course, merely a verification that our derivation of the quantities δw_ν and δw_ϕ is correct. However, in what follows, when the magnetic field is not dipolar, the comparison of the computed cross-sectional area with the magnetic field is a valuable method of checking the accuracy of the method of computation.

3 Field mapping in general models of the magnetic field

Mathematical models of the geomagnetic field are now available that not only provide for a good fit to the Earth's interior field, but also allow for the various exterior current systems arising from the interaction of the solar wind and the magnetosphere. The IGRF is a spherical harmonic representation of the interior field (Maus et al., 2005) while Tsyganenko (1987, 1995, 1996) has used solar wind data to determine appropriate parameters for the exterior field model where each contribution is given by appropriate polynomials of the coordinate system with the coefficients determined by the solar wind conditions. In such a model the magnetic field is specified everywhere as a function of position

$$\boldsymbol{B} = \boldsymbol{B}(\boldsymbol{r}), \quad (40)$$

where $\boldsymbol{r}$ is the position.

We discuss the mapping of electric fields along field lines in such a model. It is not the intention of this paper to perform detailed calculations in the various realistic models; this will be left to a future paper. We discuss only the principles with illustrative calculations in a simplified model.

In what follows we use vector notation and Cartesian tensor notation (eg Walker, 2005, Appendix A1) interchangeably as convenient. A subscript i takes the values (1,2,3) representing the three Cartesian components of a vector. Second rank Cartesian tensors have two subscripts. A repeated suffix implies summation. Consider a field line originating at a point located at a radius r_i. An adjacent point on the field line is at $r_i + \delta r_i$ where the magnitude of δr_i is δs. The notation is that differences δ represent the difference between quantities measured on the adjacent field lines, while differences Δ arise as a consequence of moving along the field line.

The unit vector parallel to the field line is

$$\frac{\mathrm{d}r_i(s)}{\mathrm{d}s} \equiv \hat{\mu}_i = \frac{B_i}{B}. \quad (41)$$

If the magnetic field is defined throughout space this is a set of three first order simultaneous differential equations for the field line. They can be integrated numerically step by step using a Runge-Kutta or other suitable process.

Now consider a field line passing through some point in space that is taken as the origin as shown in Fig. 3a. At a point A, distance s along the field line, the unit vector $\hat{\boldsymbol{\mu}} \equiv \boldsymbol{B}/B$ is directed parallel to the field line. An adjacent field line passes through point B, displaced, normal to $\hat{\boldsymbol{\mu}}$, by a small amount $w_i^\perp$. The adjacent field line lies along BD. Taylor's theorem shows that, to first order in $w_i^\perp$, the unit vector tangent to the second field line at B is

$$\hat{\mu}_i + \delta\hat{\mu}_i = \hat{\mu}_i + \frac{\partial\hat{\mu}_i}{\partial x_j} w_j^\perp = \hat{\mu}_i + T_{ij} w_j^\perp, \quad (42)$$

where

$$T_{ij} \equiv \frac{\partial\hat{\mu}_i}{\partial x_j}. \quad (43)$$

Note that unit vectors can only change direction not magnitude. Since $\hat{\mu}_i$ is a unit vector, $\delta\hat{\mu}_i$ is normal to it, and has components parallel and perpendicular to $w_i^\perp$. The parallel component arises from the divergence of the two field lines while the perpendicular component is the consequence of shear of the field lines.

If we now advance a small distance Δs from A to C and from B to D the separation of the adjacent field line is $w_i^\perp + \Delta w_i^\perp$. In the diagram AC and BE are parallel and of length

Table 1. Mapping of the convective drift from the ionosphere at height h_1 to DMSP altitude $h_2 = 840$ km along dipole field lines of varying L. The ratio of the eastward (ϕ) components (column 2) does not change with L. The ratio of velocity components v_ν in the magnetic meridian plane is given for various L.

h_1 (km)	$v_{\phi,2}/v_{\phi,1}$ (all L)	$v_{\nu,2}/v_{\nu,1}$ $L = 6.6$	$v_{\nu,2}/v_{\nu,1}$ $L = 6.0$	$v_{\nu,2}/v_{\nu,1}$ $L = 5.5$	$v_{\nu,2}/v_{\nu,1}$ $L = 5.0$	$v_{\nu,2}/v_{\nu,1}$ $L = 4.5$	$v_{\nu,2}/v_{\nu,1}$ $L = 4.0$	$v_{\nu,2}/v_{\nu,1}$ $L = 3.0$
350	1.1112	1.1168	1.1174	1.1181	1.1189	1.1199	1.1213	1.1260
300	1.1237	1.1299	1.1306	1.1314	1.1323	1.1334	1.1350	1.1402
250	1.1365	1.1433	1.1441	1.1449	1.1459	1.1472	1.1489	1.1546
200	1.1494	1.1569	1.1578	1.1587	1.1598	1.1612	1.1631	1.1694
150	1.1627	1.1708	1.1718	1.1728	1.1740	1.1755	1.1775	1.1827
100	1.1762	1.1850	1.1860	1.1871	1.1884	1.1901	1.1923	1.1997

Δs. The distance BG is also of length Δs. If we were to move from point B a distance Δs in a straight line along the direction of $\hat{\boldsymbol{\mu}}$ we would reach the point E while along the direction of $\hat{\boldsymbol{\mu}} + \delta\hat{\boldsymbol{\mu}}$ we would reach G. The displacement from E to G is $\delta \boldsymbol{w}_\perp$ and results from the divergence and shear of the field lines. Clearly, since the magnitude of $\hat{\boldsymbol{\mu}}$ is unity,

$$\frac{\delta w_i^\perp}{\Delta s} = \frac{\delta \hat{\mu}_i}{1} = T_{ij} w_j^\perp. \tag{44}$$

The vector $\boldsymbol{w}_\perp + \delta \boldsymbol{w}_\perp$ is not, however, perpendicular to the field line at C because of the curvature. It must be rotated to point D to coincide with $\boldsymbol{w}_\perp + \Delta \boldsymbol{w}_\perp$. The definition of the field line curvature is illustrated in Fig. 3b (Walker, 2005, Appendix B.2). A small arc of length Δs on the field line subtends an angle ϕ at the centre of curvature. The unit vector $\hat{\mu}_i$, tangent to the field line rotates along the arc through the same angle ϕ. In the limit $\phi \to 0$, $\Delta\hat{\mu}_i$ is normal to $\hat{\mu}_i$. The curvature $\boldsymbol{\kappa}$ is defined as a vector of magnitude $1/R$ directed towards the centre of curvature. Clearly, in the limit of small ϕ,

$$\phi = \frac{\Delta\hat{\mu}}{1} = \frac{\Delta s}{R} \tag{45}$$

so that

$$\boldsymbol{\kappa} = \frac{d\hat{\boldsymbol{\mu}}}{ds} = (\hat{\boldsymbol{\mu}}.\nabla)\hat{\boldsymbol{\mu}} \Rightarrow \hat{\mu}_j T_{ij}. \tag{46}$$

As shown in Fig. 3c $\boldsymbol{\kappa}$ makes an angle θ with $\boldsymbol{w}_\perp$. The component of $\boldsymbol{w}_\perp$ along $\boldsymbol{\kappa}$ is the scalar product of $\boldsymbol{w}_\perp$ and the unit vector $\hat{\boldsymbol{\kappa}}$. It is positive when θ is an acute angle and negative when it is obtuse. The vector $\delta \boldsymbol{s}$ is then given by

$$\frac{\delta \boldsymbol{s}}{\hat{\boldsymbol{\kappa}}.\boldsymbol{w}_\perp} = -\hat{\boldsymbol{\mu}} \frac{\Delta s}{R} \tag{47}$$

or, in subscript notation

$$\frac{\delta s_i}{\Delta s} = -\hat{\mu}_i \frac{\hat{\kappa}_j w_j^\perp}{R} = -\hat{\mu}_i \kappa_j w_j^\perp = -\hat{\mu}_i \hat{\mu}_k T_{jk} w_j^\perp. \tag{48}$$

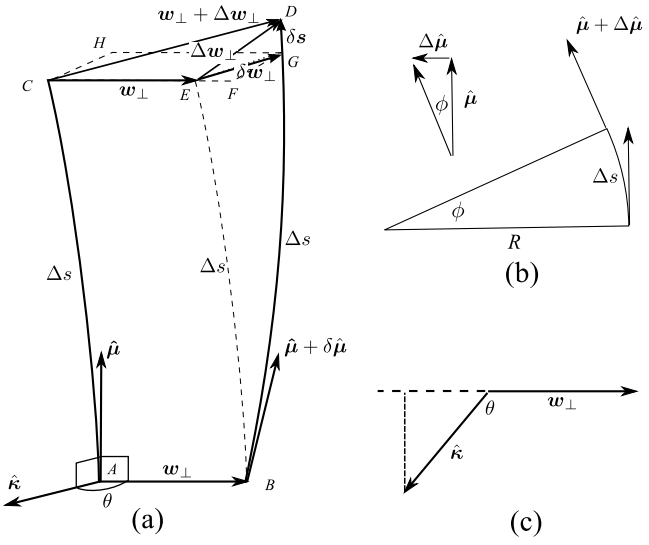

Figure 3. Definition of T_{ij}. **(a)** Relative displacement of adjacent field lines; **(b)** Field line curvature; **(c)** Component of $\boldsymbol{w}_\perp$ along curvature vector.

The elements of T_{ij} are given by

$$\begin{aligned} T_{ij} &= \frac{\partial \hat{\mu}_i}{\partial x_j} = \frac{\partial}{\partial x_j}\left(\frac{B_i}{B}\right) \\ &= \frac{1}{B}\left\{\frac{\partial B_i}{\partial x_j} - \frac{B_i}{B}\frac{\partial B}{\partial x_j}\right\} \\ &= \frac{1}{B}\left\{\delta_{ik} - \frac{B_i B_k}{B^2}\right\}\frac{\partial B_k}{\partial x_j} \end{aligned} \tag{49}$$

and the components of **B** and its derivatives may be found from the model. Finally

$$\Delta w_i^\perp = \delta w_i^\perp + \delta s_i \tag{50}$$

so that, from Eqs. (44) and (48)

$$\frac{dw_i^\perp}{\mathrm{d}s} = T_{ij} w_j^\perp - \hat{\mu}_i \hat{\mu}_l T_{kl} w_k^\perp. \tag{51}$$

The differential width $w_i^\perp$ can be normalized to its initial value so that, at $s = 0$, $w_i^\perp(0)$ is a unit vector in the direction

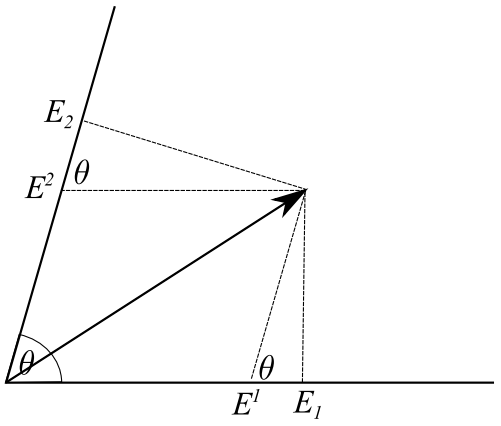

Figure 4. Covariant and contravariant components of $\boldsymbol{E}$.

of the electric field. To map a component of the electric field along a field line, Eqs. (41) and (51) can be integrated numerically to the desired end point. The mapping procedure is then as follows:

- The initial value for integrating (Eq. 51) is a unit vector in the direction of the desired component of the electric field $\boldsymbol{E}$.
- Equations (41) and (51) are integrated step by step along the field line giving the coordinates of the field line and the coordinates of the vector $\boldsymbol{w}_\perp$ as a function of distance s along the field line.
- The mapped electric field component in the direction of $\boldsymbol{w}_\perp$ at each point on the field line has magnitude $E_0/w_\perp$.
- The procedure can be carried out for two initial values of $\boldsymbol{w}_\perp$ to give two components of the field line.

Although the two initial values of $\boldsymbol{w}_\perp$ may be at right angles to each other, there is no reason to suppose that they will remain at right angles as the integration proceeds along the field line. The computation of the resultant electric field therefore requires care. In general, the directions of the two values of $\boldsymbol{w}_\perp$ define a set of two-dimensional oblique coordinates as shown in Fig. 4. The two components of $\boldsymbol{E}$ that have been calculated are E_1 and E_2, the *covariant* components in the oblique system. To calculate the resultant $\boldsymbol{E}$ we need the *contravariant* components given by

$$E^1 = \frac{E_1 - E_2\cos\theta}{\sin^2\theta} \quad (52)$$

$$E^2 = \frac{-E_1\cos\theta + E_2}{\sin^2\theta}, \quad (53)$$

as can be seen from the figure. The resultant $\boldsymbol{E}$ is calculated from these using the parallelogram rule.

4 A simple night-side model

4.1 Characteristics of the model

We illustrate the use of the first order differential Eqs. (41) and (51). We use a right-handed CGM coordinate system with origin at the centre of the Earth, x directed towards the Sun, y from dawn to dusk and z northward along the axis. The magnetic field is a dipole field with the addition of a Harris (1962) current sheet to represent the tail. The magnetic field components are then given by

$$B_x = -\frac{3B_{\rm eq}R_{\rm E}^3 xz}{(x^2+y^2+z^2)^{5/2}} + B_{\rm h}\tanh\frac{z}{d} \quad (54)$$

$$B_y = -\frac{3B_{\rm eq}R_{\rm E}^3 yz}{(x^2+y^2+z^2)^{5/2}} \quad (55)$$

$$B_z = \frac{B_{\rm eq}R_{\rm E}^3(x^2+y^2-2z^2)}{(x^2+y^2+z^2)^{5/2}}, \quad (56)$$

where the last term in Eq. (54) arises from a Harris cross tail current. This model is not over-complicated and gives qualitatively realistic magnetic fields on the night side.

The derivatives of the components of **B** are then

$$\frac{\partial B_x}{\partial x} = \frac{3B_{\rm eq}R_{\rm E}^3 z(4x^2-y^2-z^2)}{(x^2+y^2+z^2)^{7/2}} \quad (57)$$

$$\frac{\partial B_x}{\partial y} = \frac{15B_{\rm eq}R_{\rm E}^3 xyz}{(x^2+y^2+z^2)^{7/2}} \quad (58)$$

$$\frac{\partial B_x}{\partial z} = \frac{3B_{\rm eq}R_{\rm E}^3 x(-x^2-y^2+4z^2)}{(x^2+y^2+z^2)^{7/2}} + \frac{B_t}{w}\mathrm{sech}^2\frac{z}{d} \quad (59)$$

$$\frac{\partial B_y}{\partial x} = \frac{15B_{\rm eq}R_{\rm E}^3 xyz}{(x^2+y^2+z^2)^{7/2}} \quad (60)$$

$$\frac{\partial B_y}{\partial y} = \frac{3B_{\rm eq}R_{\rm E}^3 z(-x^2+4y^2-z^2)}{(x^2+y^2+z^2)^{7/2}} \quad (61)$$

$$\frac{\partial B_y}{\partial z} = \frac{3B_{\rm eq}R_{\rm E}^3 y(-x^2-y^2+4z^2)}{(x^2+y^2+z^2)^{7/2}} \quad (62)$$

$$\frac{\partial B_z}{\partial x} = \frac{3B_{\rm eq}R_{\rm E}^3 x(-x^2-y^2+4z^2)}{(x^2+y^2+z^2)^{7/2}} \quad (63)$$

$$\frac{\partial B_z}{\partial y} = \frac{3B_{\rm eq}R_{\rm E}^3 y(-x^2-y^2+4z^z)}{(x^2+y^2+z^2)^{7/2}} \quad (64)$$

$$\frac{\partial B_z}{\partial z} = \frac{3B_{\rm eq}R_{\rm E}^3 z(-3x^2-3y^2+2z^2)}{(x^2+y^2+z^2)^{7/2}}. \quad (65)$$

These can be used in Eq. (51) which can then be integrated simultaneously with Eq. (41). The components of the unit vector found from this, together with the magnitude of E found from Eq. (2) gives the electric field at all points along the field line. For tests of the process the Harris field $\boldsymbol{B}_{\rm h}$ can be set to zero, so that the integration of the differential equations applies to a dipole magnetic field, and the results can be compared with the explicit formulae of Sect. 2.

4.2 Mapping of electric field in the model

For our simple model we use what are effectively GSM coordinates with origin at the centre of the Earth, x towards local noon, z along the dipole axis, and y completing the right hand set. The field line trace can start from any point x, y, z on a field line. Normally the point would be defined by latitude, longitude and radius (or height) and converted to the rectangular system.

The initial value of $w_i^{\perp}$ must be found from the electric field. When measuring an electric field in the upper ionosphere or magnetosphere, it is only necessary to have two components. Because the component parallel to $\boldsymbol{B}$ is zero, the third component can be found from the condition $\boldsymbol{E} \cdot \boldsymbol{B} = 0$. For example if the H and D components of $\boldsymbol{E}$ are measured by a SuperDARN radar then the vertical component is given by

$$E_z = -\frac{B_H E_H + B_D E_D}{B_z}. \tag{66}$$

Let τ be the local time measured in hours. Then the longitude ϕ measured from noon (i.e. from the positive x axis) is given by

$$\phi = \left(\frac{\tau}{12} - 1\right)\pi. \tag{67}$$

Then the direction cosines of the H and D directions are

$$\hat{n}_i^{\lambda} = \{-\sin\lambda\cos\phi, -\sin\lambda\sin\phi, \cos\lambda\} \tag{68}$$

$$\hat{n}_i^{\phi} = \{-\sin\phi, \cos\phi, 0\} \tag{69}$$

and

$$\boldsymbol{E} = \hat{\boldsymbol{n}}_{\lambda} E_H + \hat{\boldsymbol{n}}_{\phi} E_D + \hat{\boldsymbol{z}} E_z. \tag{70}$$

It should be noted that, if all three components of $\boldsymbol{E}$ are given, they must be normal to the magnetic field. The differential Eqs. (51) assume this and if it is not true, there will be a cumulative error in the integration.

The starting value for $\boldsymbol{w}_{\perp}$ is then the unit vector

$$\boldsymbol{w}_{\perp}(0) = \frac{\hat{\boldsymbol{n}}_{\lambda} E_H + \hat{\boldsymbol{n}}_{\phi} E_D + \hat{\boldsymbol{z}} E_z}{\sqrt{E_x^2 + E_y^2 + E_z^2}}. \tag{71}$$

5 Computational results

5.1 Dipole field: comparison with explicit formulae

An initial test of the method is to use Eqs. (41) and (51) to trace field lines in a dipole magnetic field and compare the results with the explicit formulae of Sect. 2. We set $\boldsymbol{B}_{\mathrm{h}} = 0$ in Eqs. (54) and (59) and used a straightforward 4th order Runge-Kutta method similar to that of Press et al. (1989, Sect. 15.1) to integrate the equations. With an appropriate choice of step length, all computed values agreed with the analytic values to within the numerical accuracy of the integration process. For example Fig. 5 compares the field line separation in the magnetic meridian (full line) with that computed from Eq. (18) (crosses) for a field line starting at 72° at a height of 250 km in the ionosphere and finishing at the equatorial plane. The results agree to better than 1 part in 10^6 for an integration step length of 1 R_{E}.

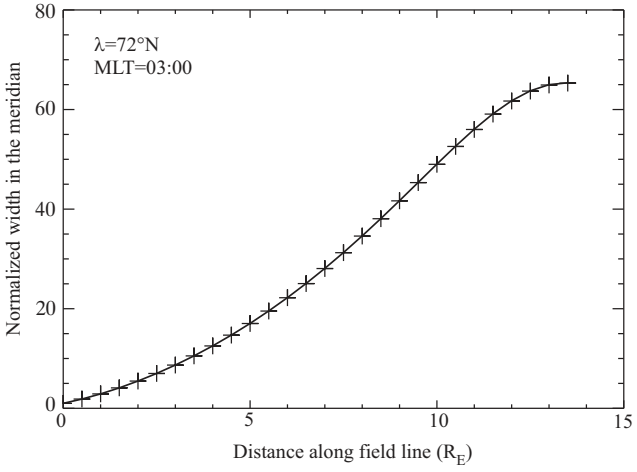

Figure 5. Element of field line separation in the meridian plane for a dipole magnetic field, normalized to the value at the Earth's surface. The full line shows the values obtained by integrating the first order differential equations, while the crosses are obtained from the analytic expression.

5.2 Electric field mapping in the Harris model

We have tested the validity of the method of field line mapping that is described in Sect. 3 by using the Harris model. The coding is in Python with the intention of providing a template for an open source package that will be developed for electric field mapping in more realistic magnetic field geometries (Maus et al., 2005; Tsyganenko, 1987, 1995, 1996).

The integration process is the same as described above for a dipole. The results for the field line coordinates x_i and normalized separation w_i are stored in arrays. If we wish to terminate at a particular point we specify a function of s, the distance along the field line that must be zero at the end point. When this function changes sign we take the coordinates of the last two points as the starting values for a *regula falsi* (Press et al., 1989) process to find the zero of the function. For example, if we choose to end the trace in the ionosphere at an altitude of 250 km we evaluate $h - 250$ at each point along the path. When it changes sign we enter the *regula falsi* routine. This interpolates linearly between the last two values s_1 and s_2 of s to find a new value s_3 that is closer to the root. With a step length of $s_3 - s_2$ the equations are advanced another step to find a new h. This is repeated until $|h - 250| \leq \epsilon$ where ϵ is small enough to give the required accuracy. Although this is a first order convergent process

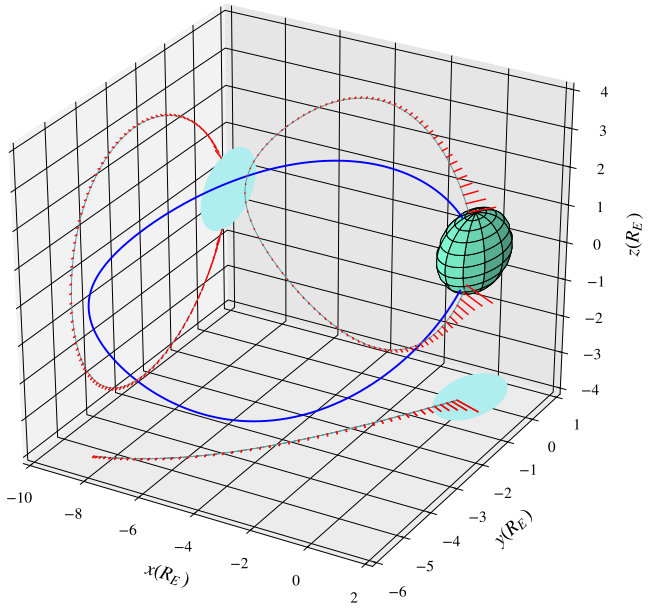

Figure 6. Field line trace (blue) and electric field mapping (red) in a Harris model with $B_{eq} = 3.4 \times 10^4$ nT, $B_0 = 50.0$ nT and plasma sheet thickness $d = 1.5 R_E$. The trace starts at 70° latitude, 03:00 LT (local time), and 250 km altitude. The projections of the magnetic field line and the electric field vectors on the coordinate planes are also shown. Scale of electric field vector: 1 length unit = 35.4 mV m^{-1}.

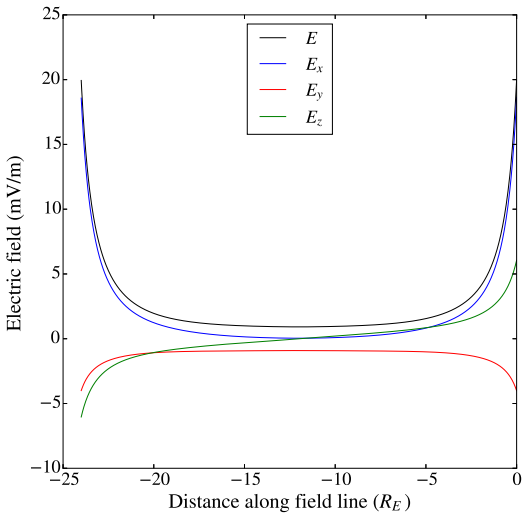

Figure 7. Electric field normalized to the value at the starting point, for the field line traced and electric field mapped in Fig. 6.

and converges more slowly than a second order process such as the Newton-Raphson method, it requires much less computation. In practice it only requires about five or six steps to achieve an accuracy of one part in 10^6.

Figure 6 shows the results of such a process. A field line is traced from a point in the Northern Hemisphere ionosphere at altitude 250 km, latitude 70° and local time 03h00. The parameters of the model (shown in the caption) are chosen to produce a strong tail field. The trace is terminated at an altitude of 250 km in the opposite hemisphere. The model is, of course, symmetric about the equatorial plane. The blue line represents the magnetic field line. The effect of the Harris sheet is obvious, with the field line being swept back tailwards and strong curvature within the plasma sheet. We also show the projection of the field line on each of the coordinate planes. The electric field is represented by the red line segments along the field line projections. Each line segment represents the projection of the electric field vector on the coordinate plane.

Because there is strong dependence of the electric field magnitude on radius the field vectors are barely discernable at larger radii. The diagram is not, however, intended to provide a quantitative picture of the electric field mapping but to give a feel for the geometry. A better idea of the variation of $\boldsymbol{E}$ along the field line is given in Figs. 7 and 8. Figure 7 shows magnitude of the electric field and of its three components as a function of s, the distance measured along the field line (negative when in the opposite direction to $\boldsymbol{B}$). The x and y components of $\boldsymbol{E}$ are symmetric about the equator while E_z is antisymmetric. There is strong variation of the magnitude of E, which varies from 35.4 mV m^{-1} in the ionosphere to about 0.5 mV m^{-1} near the equator. A better idea of how $\boldsymbol{E}$ varies near the equator can be obtained by examining Fig. 8. The normalized width vector is in the same direction as $\boldsymbol{E}$ and its magnitude is proportional to the reciprocal of E.

It is not the intention of this paper to provide the results of a large number of computations in a model that is only intended to be illustrative. The purpose is to validate the technique of computation in a relatively simple model. We describe below the various checks that we have made on the accuracy of the integration technique.

5.3 Computational checks of mapping in the Harris model

We have already described how, in a dipole model, we can use the integration technique and compare the results with the explicit formulae presented in the first part of the paper. The agreement is, in all cases, very good. With integration steps of 1.5 to 2.0 R_E agreement between the computed values of position x_i and field line separation w_i/w_0 is typically about 1 part in 10^6 for a dipole model. Larger steps than this increase the truncation error and reduce the accuracy. The step length is best chosen by the user to suit the numerical accuracy of the computer and the requirements of the problem.

In the Harris model the curvature of the field lines near the plasma sheet can be quite large. If the step length is comparable with the radius of curvature, truncation error becomes important. In this case the orthogonality of $\boldsymbol{w}$ and $\boldsymbol{B}$ is not

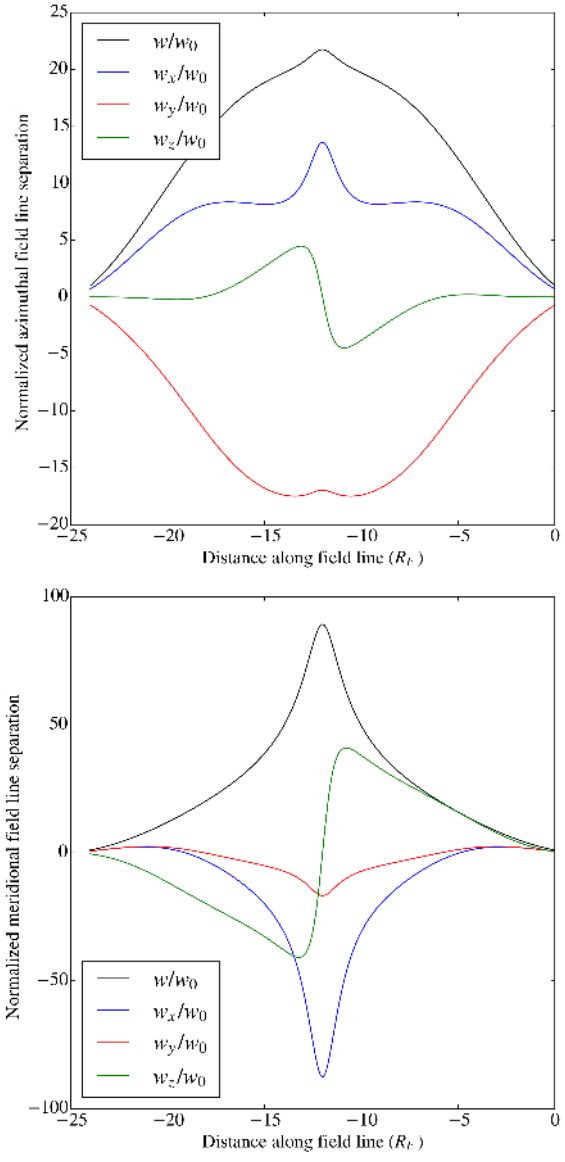

Figure 8. Element of field line separation in the electric field direction, for the field line traced in Fig. 6.

maintained. As a check against this, at each step, we calculate the scalar product of the unit vectors parallel to $\boldsymbol{w}$ and $\boldsymbol{B}$. If its magnitude exceeds a predetermined value an exception is raised and the user can set a better step length. Ultimately, in production versions of the program for realistic models it will be necessary to use a more sophisticated adaptive step integration technique. For the present the simpler technique suffices.

Another check that will be particularly useful in more elaborate models is to take two initial values of $\boldsymbol{w}$, $\boldsymbol{w}_1$ and $\boldsymbol{w}_2$, in different directions perpendicular to $\boldsymbol{B}$. These can both be integrated simultaneously along the field line. Then the cross-section of the flux tube defined by these is $\boldsymbol{w}_1 \times \boldsymbol{w}_2$. The magnetic flux is constant along the flux tube and we can check this by evaluating $\boldsymbol{B} \cdot \boldsymbol{w}_1 \times \boldsymbol{w}_2$ at each step. In an integration in the Harris model constancy can be maintained to about 1 part in 10^6 with appropriate step length. The computational overhead of integrating three additional equations is too large for this to be useful in routine calculations, but it is very useful in checking the correctness of the coding for the magnetic field model.

6 Discussion and conclusions

In this paper we have introduced a new method of mapping electric fields along geomagnetic field lines. A set of three differential equations for the components of the normalized separation of two field lines has been obtained. These can be integrated simultaneously with the equations that trace the field line. Since the magnetic field lines are equipotentials, this allows the calculation of a component of the electric field as a function of distance measured along the field line. Two values of the normalized separation are required to give two field line components resulting in a total of nine first order differential equations that must be simultaneously integrated.

The computational effort in integrating the set of nine equations is the same as that for tracing three field lines. The accuracy of the process is better, however, since finding the electric field by finding the difference between the end positions of the two field lines requires taking small differences of large quantities. Such numerical differentiation is notoriously inaccurate.

The viability of the method has been carefully tested. The analytic expressions for a number of relevant properties of a magnetic dipole field, while easily derived, are not readily available in the literature. We have provided a derivation of these for convenient reference and compared the results calculated from them with those obtained by the integration method. We have also tested the method in a qualitatively more realistic model of the night side magnetosphere. All the tests show that the method is accurate and suitable for mapping in more realistic models. In the accompanying paper (Walker, 2016) the process is applied to the International Geomagnetic Reference Field.

Acknowledgements. This work was supported by the South African National Research Foundation under grant 93068 (SANAE HF Radar), and by the University of KwaZulu-Natal through a research incentive grant.

The topical editor, E. Roussos, thanks J. M. Ruohoniemi and one anonymous referee for help in evaluating this paper.

References

Baker, J. B. H., Greenwald, R. A., Ruohoniemi, J. M., Forster, M., Paschmann, G., Donovan, E. F., Tsyganenko, N. A., Quinn, J. M., and Balogh, A.: Conjugate comparison of Super Dual Auroral Radar Network and Cluster electron drift instrument measurements of E × B plasma drift, J. Geophys. Res., 109, A01209, doi:10.1029/2003JA009912, 2004.

Greenwald, R. A., Baker, K. B., Dudeney, J. R., Pinnock, M., Jones, T. B., Thomas, E. C., Villain, J.-P., Cerisier, J.-C., Senior, C., Hanuise, C., Hunsucker, R. D., Sofko, G., Koehler, J., Nielsen, E., Pellinen, R., Walker, A. D. M., Sato, N., and Yamagishi, H.: DARN/SuperDARN: A global view of high latitude convection, Space Sci. Rev., 71, 761–796, 1995

Harris, E. G.: On a plasma sheath separating regions of oppositely directed magnetic field, Nuovo Cimento, 23, 115–121, 1962.

Lyons, L. R. and Williams, D. J.: Quantitative Aspects of Magnetospheric Physics, D. Reidel Publishing Company, Dordrecht, Holland, 231 pp., 1984.

Maus, S., Macmillan, S., Chernova, T., Choi, S., Dater, D., Golovkov, V., Lesur, V., Lowes, F., Luhr, H., Mai, W., McLean, S., Olsen, N., Rother, M., Sabaka, T., Thomson, A., and Zvereva, T.: The 10th-Generation International Geomagnetic Reference Field, Geophys. J. Int., 161, 561–565, 2005.

Mozer, F. S.: Electric field mapping from the ionosphere to the equatorial plane, Planet. Space Sci., 18, 259–263, 1970.

Press, W. H., Flannery, B. P., Teukolsky, S. A., and Vetterling, W. T.: Numerical Recipes, (FORTRAN version or Pascal version or C version), Cambridge University Press, Cambridge, 818 pp., 1989.

Tsyganenko, N. A.: Global quantitative models of the geomagnetic field in the cislunar magnetosphere for different disturbance levels, Planet. Space Sci., 35, 1347–1358, 1987.

Tsyganenko, N. A.: Modeling the Earth's magnetospheric magnetic field confined within a realistic magnetopause, J. Geophys. Res., 100, 5599–5612, 1995.

Tsyganenko, N. A.: Effects of the solar wind conditions on the global magnetospheric configuration as deduced from data-based field models, European Space Agency Publication ESA SP-389, p. 181, 1996.

Walker, A. D. M.: Magnetohydrodynamic Waves in Geospace: The theory of ULF waves and their interaction with energetic particles in the solar-terrestrial environment, IOP Press, Bristol, UK, 549 pp., 2005.

Walker, A. D. M.: Mapping of steady-state electric fields and convective drifts in geomagnetic fields – Part 2: The IGRF, Ann. Geophys., 34, 67–73, doi:10.5194/angeo-34-67-2016, 2016.